**Light Metals 2015**
*Edited by: Margaret Hyland*
***TMS (The Minerals, Metals & Materials Society), 2015***

# INFLUENCE OF TEMPERATURE ON NATURAL AGING KINETICS OF AA6061 MODIFIED WITH Sn

Marion Werinos[1], Helmut Antrekowitsch[1], Werner Fragner[2], Thomas Ebner[2], Peter J. Uggowitzer[3], Stefan Pogatscher[3]
[1]Chair of Nonferrous Metallurgy, Montanuniversitaet Leoben; Franz-Josef-Straße 18, Leoben 8700, Austria
[2]AMAG Austria Metall AG; Lamprechtshausenerstrasse 61, Braunau-Ranshofen 5282, Austria
[3]Laboratory of Metal Physics and Technology, ETH Zurich; Vladimir-Prelog-Weg 4, Zurich 8093, Switzerland

Keywords: aluminum alloys, natural aging, vacancies, trace elements, solution heat treatment

## Abstract

Al-Mg-Si alloys are widely used in cast, wrought and extruded form. A characteristic property of these alloys is the negative effect of natural pre-aging at room temperature on artificial aging. Minor additions of Sn suppress the adverse effect of room temperature aging due to controlled buffering of quenched-in excess vacancies at low temperatures. In this study we evaluate the buffering performance of Sn in the temperature range between 5 and 45 °C. This is investigated for two Sn-added AA6061 alloys with systematic variation in their Mg-, Si- and Cu-content, for comparison the natural aging kinetics of a Sn-free alloy is studied. In general a strong dependence of hardening kinetics on temperature and on chemical composition is observed. Results of aging kinetics are discussed in terms of common clustering theories and the temperature dependent trapping effect of Sn on excess vacancies.

## Introduction

Today numerous age hardenable Al-Mg-Si alloys are used as structural materials in cast, wrought, rolled or extruded form in the automotive, shipbuilding, architecture, and aviation industry [1–4]. Rich alloys like AA6061 show a strong adverse influence of natural aging (NA) on subsequent artificial aging (AA). This negative effect appears within minutes of room temperature (RT) storage after quenching from solution treatment temperatures (STT) ~800 K [4,5]. During AA at commonly 150 to 180 °C, NA retards the hardening kinetics by an order of magnitude and reduces the achievable strength. Since discovered 75 years ago [6] many researchers have addressed this problem [2,4,7,8]. Still, the exact mechanisms remain unsolved.

Recently, the origin of the negative effect on AA has been linked to the clustering processes at RT [2]. The simple concept assumes that clusters formed during NA act as traps for quenched-in thermal vacancies during AA. Largely dependent on the thermal stability of these clusters, vacancies may be released and become mobile again. Due to the slow dissolution kinetics of these clusters at typical AA temperatures, clusters act as stable vacancy prisons during AA. Hence, a reduced contribution of quenched-in vacancies to diffusion during the nucleation of the major hardening phase β'' [9] can explain the negative effect of NA on AA [10].

Recently we presented a concept which avoids the formation of clusters at RT by adding trace amounts of the element Sn to the alloy AA6061 leading to the suppression of hardening during NA for > 2 weeks after a solution heat treatment (SHT) at 570 °C and water-quenching to RT [3,11]. Without Sn, NA starts already after several minutes. The slowdown of NA kinetics is achievable in principle by suppressing vacancy diffusion at RT while allowing such diffusion during processing at elevated temperature (e.g. AA) [3]. Sn exhibits a high binding energy $\Delta E_{SV}$ to vacancies of 0.24 eV (calculated for Sn-vacancy pairs using quantum DFT [3]). This results in trapping of vacancies in preferably Sn-vacancy pairs which strongly retards the formation of clusters. Thus, temporary suppression of NA at RT is achieved.

Further research revealed an influence of STT and composition on the achievable retardation of age hardening during NA [11]. To quantify the retarding effect of Sn on NA in AA6061 we proposed the retardation factor $R = 1 + 12c_{Sn}(e^{\Delta E_{SV}/kT})$ (Equation 1, [3]) which is also useful to understand the influence of STT and composition. $c_{Sn}$ is the concentration of Sn in fcc Al, $k$ is Boltzmann's constant. The Sn-vacancy pairs, formed during or after quenching from STT to RT, buffer vacancies during NA, which leaves fewer untrapped vacancies available for diffusion of other alloying atoms such as Mg or Si. Thus NA kinetics is slowed down through the reduction of mobile vacancies in the matrix. Investigation of STTs in the range of 570 °C to 510 °C, revealed an earlier onset of NA-hardening at lower STT [11]. As obvious from Equation 1, the retardation of NA depends linearly on $c_{Sn}$. For the STT applied, it is assumed that the total amount of solute Sn dissolved in fcc Al at STT complies with the equilibrium level. A significant reduction of $c_{Sn}$ due to decreasing solubility at lower STT can explain why the effect of Sn on NA kinetics is reduced. A similar effect on $c_{Sn}$ was found for a variation of the Si-content [11]. Confirmed by thermodynamic calculations, an increasing Si-content from 0.6 wt.% to 0.8 wt.% in AA6061 reduces $c_{Sn}$ at the annealing temperature of 570 °C and thus the RT stability of the alloy. A small variation of the Mg- and Cu-content showed only small effects on NA kinetics. Atom probe tomography measurements revealed a maximum Sn-solubility of ~100 at. ppm after quenching from 570 °C for the AA6061 alloy investigated in Ref. [3] (alloy 2 in Table 1). For Sn additions above this solubility limit no further retardation of hardening is achievable. Sn-contents below the solubility limit exhibit an earlier onset of hardening [3].

The present work investigates the influence of varying NA temperature on kinetics using hardness measurements. Seyedrezai et al. [12] studied this phenomenon between -20 and 50 °C for the alloy Al-0.5%Mg-1%Si applying electrical resistivity measurements and positron annihilation spectroscopy. The authors identified three stages of clustering indicated by three extended periods of time, over which the resistivity increases linearly with the logarithm of time. At higher NA temperatures, i.e. 20 °C and 50 °C, only the last two stages have been observed during the aging times investigated. Applying the cross-cut technique, the evaluation of the activation energy of clustering $Q$ for the second stage revealed ~45 kJ/mol [12], which is interpreted to be related to the energy of migration of a Mg-vacancy pair with ~49 kJ/mol [13]. By computing the approximate diffusion distances of solutes for the transition from stage II to III using migration activation energies of Mg and Si,

they obtained constant diffusion distances. Thus, the transition from stage II to III is associated to be related to the impingement of the solute fields around clusters [12]. Further, Seyedrezai et al. [12] found a relatively small influence of a change in the STT on NA kinetics and thus on the activation energy $Q$. This was interpreted as a confirmation that the mechanism of clustering remains unchanged. According to [14,15] this can be explained by finding that the temperature at which the vacancy concentration is frozen in, is generally much lower than the STT.
Here we show a significant influence of not only the NA temperature, but also an effect of the STT on NA kinetics with and without Sn-addition in a commercial AA6061 alloy. An estimation of the effective activation energy of clustering $Q$ indicates a significant influence of Sn-addition.

## Experimental

Alloy 1 (Table 1) was prepared by melting an industrially produced AA6061 alloy followed by die-casting. Alloys 2 and 3 (Table 1) were produced from an AA6061 base alloy, already containing ~95 at. ppm Sn (as well as Mg 0.80, Si 0.59, Cu 0.21, Fe 0.47, Cr 0.15, Mn 0.12, Zn 0.05 and Ti 0.04, all in wt.%), which was produced by the Austrian Institute of Technology (AIT) in Ranshofen (Austria) using a continuous caster in laboratory scale. The Sn content of 95 at. ppm complies with the solubility limit in alloy 2 at 570 °C (see introduction). To obtain the compositions listed in Table 1, the base alloy was re-melted and Mg, Si and Cu were added accordingly. After alloying, Ar gas purging was applied to reduce the hydrogen content before the alloys were cast to slabs (150 × 90 × 35 $mm^3$). After cutting and homogenization, hot rolling from 20 to 4.2 mm thickness was conducted. To check the chemical composition, optical emission spectrometry (SPECTROMAXx from SPECTRO) was performed on the final plates using an appropriate calibration sample for Al-Mg-Si alloys as standard (Mg 0.85, Si 1.00, Cu 0.08, in wt.%). Hardness test samples (17 × 10 × 4 $mm^3$) were solution heat treated in a circulating air furnace (Nabertherm N60/85 SHA) at different temperatures (530 °C or 570 °C) for 20 min. Subsequent quenching was carried out in water at RT and samples were kept in two Peltier-cooled incubators (IPP from Memmert) at RT (25 °C) or 45 °C for NA. Samples naturally aged at 5 °C were kept in a refrigerator.
Alloy 1 in Table 1 represents the almost Sn-free reference alloy with low Mg-, Si- and Cu-content (l: low) and commercial amounts of trace elements (see also [3]). Apart from a Sn-content of ~95 at. ppm, alloy 2 is comparable to alloy 1. Alloy 3 with average Mg-, Si- and Cu-amounts (~: average) is intended to reveal the influence of these main alloying elements on the Sn-solubility (compare [11]).

Table 1: Composition of alloys

| Alloy | Symbol | Sn | Sn | Mg | Si | Cu | Al |
|---|---|---|---|---|---|---|---|
| | MgSiCu | [at.ppm] | [wt.%] | [wt.%] | [wt.%] | [wt.%] | |
| 1 | lll | 6 | 0.0026 | 0.81 | 0.62 | 0.220 | Bal. |
| 2 | lll | 95 | 0.042 | 0.78 | 0.61 | 0.210 | Bal. |
| 3 | ~~~ | 95 | 0.041 | 0.87 | 0.72 | 0.300 | Bal. |

Brinell hardness measurements (HBW 2.5/62.5) were carried out using an EMCO-Test M4 unit. A maximum standard deviation of 1.8 HBW was achieved.

## Results

Hardness measurement

The hardening curves of alloy 2 at 25 °C (Figure 1a and Figure 1b) show comparable NA kinetics as previously studied for Sn-added AA6061 alloys in [3] or [11] which, apart from higher Sn-content above the solubility limit, exhibit a similar composition. After a SHT at 530 °C (Figure 1a) the alloy preserves the as-quenched hardness of ~45.3 HBW for more than 86.4 ks. Starting before 172.8 ks (2 days) of NA at 25 °C the alloy shows a constant logarithmic hardness increase until 14 days of NA followed by another steady increase in hardness with lower gradient. NA at 5 °C significantly decreases hardening kinetics of alloy 2, i.e. hardening starts after ~14 days and the constant hardness increase ends after ~90 days. Fastest kinetics is perceived for aging at 45 °C. A steady rise in hardness could be interpolated between 8 h and 4 days.
After a SHT at 570 °C alloy 2 (Figure 1b) starts hardening after ~14 days of NA at 25 °C followed by a steady logarithmic increase until ~90 days. A third stage of lower gradient follows. For aging at 5 °C after ~130 days the onset of hardening can be observed. Fastest kinetics is again perceived for aging at 45 °C with linear hardening between less than 2 days and ~30 days and also followed by a third stage.

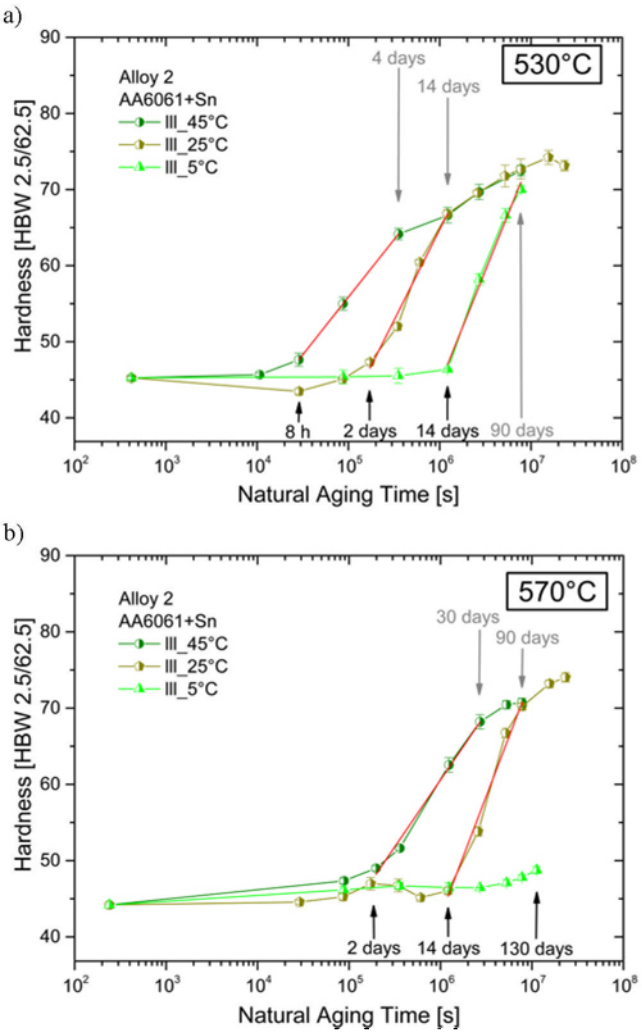


Figure 1: Influence of NA temperatures on hardening kinetics of alloy 2 after a SHT at a) 530°C and b) 570°C.

As can be seen in Figure 2 for both STTs (530 and 570 °C) and for each NA temperature (5 °C, 25 °C and 45 °C), alloy 3 exhibits faster kinetics than alloy 2 (Figure 1). For aging at 45 °C after a SHT at 530 °C (Figure 2a) three subsequent logarithmic gradients are perceived. Following the as-quenched hardness of ~46 HBW, the second stage lies between 3 h and 2 days. For aging at RT, hardening starts after ~8 h and slows down after ~14 days. At 5 °C linear hardening occurs between ~2 days and less than 60 days. After a SHT at 570 °C, NA at 45 °C leads to a linear logarithmic increase between 8 h and 4 days. During RT aging, stage II starts before 2 days and ends after ~14 days. At 5 °C the second stage is perceived between ~14 and ~133 days.

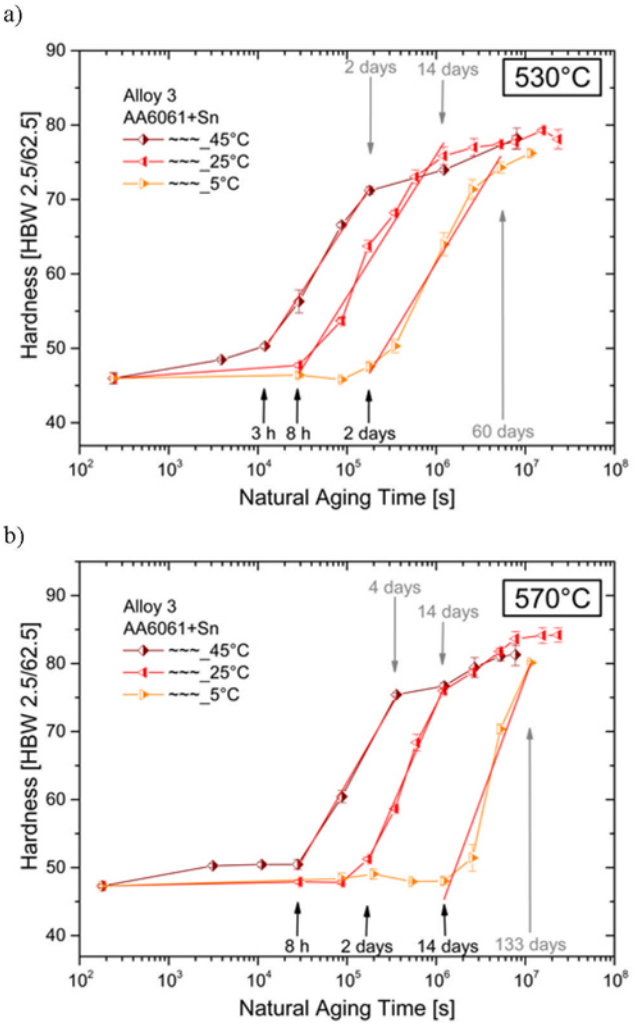


Figure 2: Influence of NA temperatures on hardening kinetics of alloy 3 after a SHT at a) 530°C and b) 570°C.

Figure 3 depicts the influence of NA temperature as well as STT on hardening kinetics of the Sn-free reference alloy 1. For 530 °C (Figure 3a) and 570 °C (Figure 3b) STT and similar NA temperatures the logarithmic hardness increase periods occur in similar aging times. At 5 °C hardening starts after ~3 h and slows down after ~14 days. At 25 °C three distinct stages are observed, the second one between 50 min and ~4 days. For aging at 45 °C only two different hardening gradients are measured. A fast logarithmic hardness increase starts at ~7 min and slows down after ~1 day, i.e. an earlier stage I of hardening is not observed at the aging times investigated.

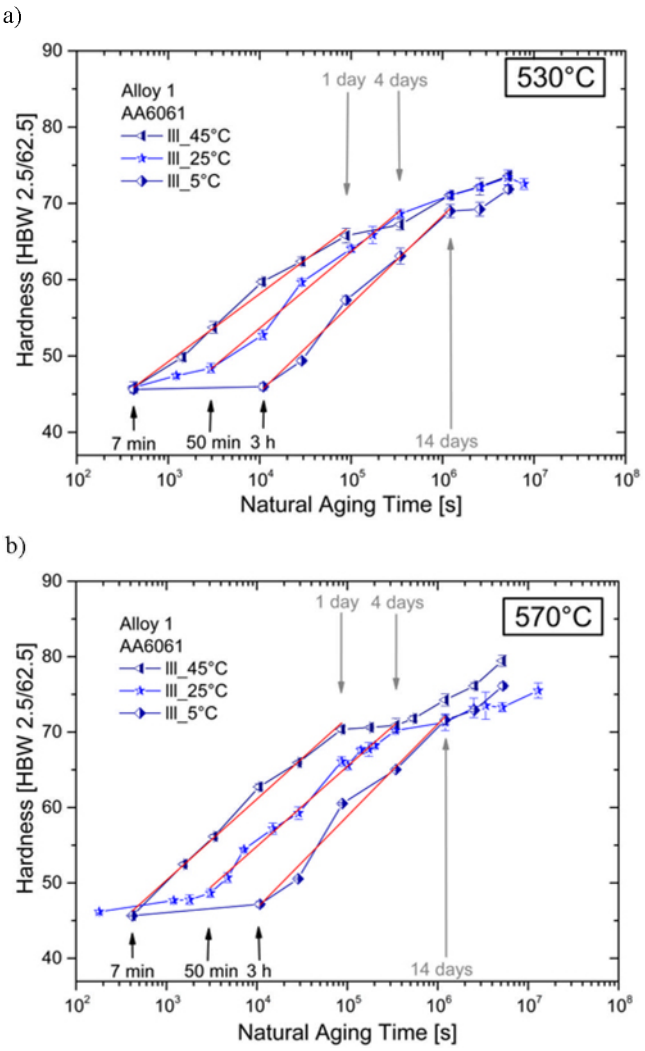


Figure 3: Influence of NA temperatures on hardening kinetics of alloy 1 after a SHT at a) 530°C and b) 570°C.

Effective activation energy calculation

Effective activation energies of clustering $Q$ are calculated using the cross-cut method as derived from Guo et at. [16] for hardness measurements and used in [12] and [17] for resistivity measurements in Al alloys. According to [16] the hardness $H$ can be expressed by the formula $H = (K_0\, exp^{(-Q/RT)}t)^n$ (Equation 2) for the clustering processes investigated. $K_0$ signifies the pre-exponential term in the Arrhenius expression for the temperature dependent rate constant $K$ (for the full equation see [16]) and $R$ is the gas constant. Taking the natural logarithm of both sides and assuming that $n$ is constant leads to $\ln 1/t = -Q/RT - \ln \Delta H_0 /n + \ln K_0$ (Equation 3). Thus the effective activation energy of clustering $Q$ can be obtained by plotting $\ln 1/t$ versus $1/T$, where $t$ is the time to reach a constant increase in hardness $\Delta H_0$ at a temperature $T$ [16]. The slope equals $-Q/R$ (see Equation 3). Preconditions for using this method are a coherent precipitate strengthening mechanism, spherical precipitates and that aging does not proceed beyond the early

stage [16]. For the calculations in the present publication, fits have been applied for the second stage of linear logarithmic hardening (Figure 1 and Figure 3) as shown in [12]. The times $t$ for the Arrhenius plot in Figure 4 are read at the same hardness value of the different curves for 5 °C, 25 °C and 45 °C. As for the calculations all curves need to be in stage II the corresponding onsets of hardening have been chosen.

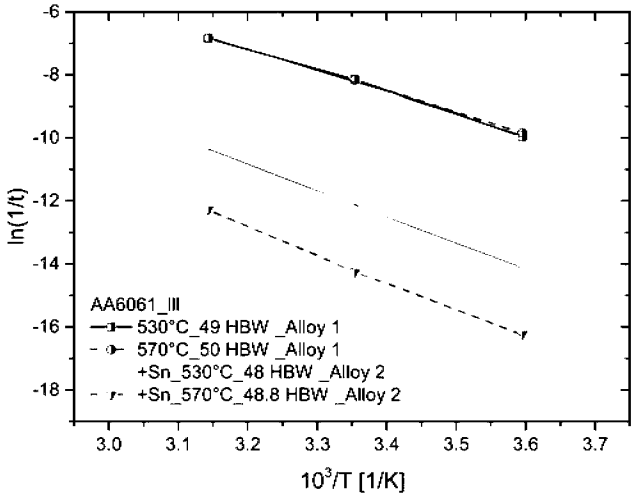


Figure 4: $\ln 1/t$ versus $1/T$ plots for the onset of hardening in stage II. The slope of the straight line equals $-Q/R$.

To evaluate the influence of Sn on the effective activation energy of clustering $Q$, Table 2 shows the calculated $Q$ values obtained for alloys 1 and 2 at the onset of hardening in stage II (see Figure 1 and Figure 3). While for alloy 1 similar activation energies $Q$ are obtained for a SHT at 530 and 570 °C, Sn-addition leads to significantly higher values at both STTs.

Table 2: Effective activation energy of clustering $Q$ for alloys 1 and 2 at a STT of 530 and 570 °C

| **Alloy** | **Symbol** | Sn | **STT** | $H_{Onset}$ | $Q$ |
|---|---|---|---|---|---|
| | MgSiCu | [at. ppm] | [°C] | [HBW] | [kJ/mol] |
| 1 | lll | 6 | 530 | 49 | 57.4 |
| 1 | lll | 6 | 570 | 50 | 55.4 |
| 2 | lll | 95 | 530 | 48 | 69.3 |
| 2 | lll | 95 | 570 | 48.8 | 72.8 |

## Discussion

The present investigation demonstrates that besides the STT and alloy composition also the NA temperature can have significant influence on the effect of Sn on NA kinetics of AA6061. Due to decreasing Sn-solubility $c_{Sn}$ at lower STT, less Sn is dissolved in fcc Al at the beginning of NA and thus the suppressive effect of Sn on NA kinetics decreases with decreasing STT. Maximum Sn-solubility (~100 at. ppm, see introduction) is obtained for alloy 2 at 570 °C and thus maximum retardation of NA is achieved (Figure 1b). The same effect of a lower $c_{Sn}$ applies for the higher Si-containing alloy 3 (see [11]). Variation of the NA temperature between 5 °C and 45 °C reveals slower hardening kinetics with lower temperatures, which applies for the Sn-free reference alloy 1 as well as the Sn-added alloys 2 and 3. Calculations of effective activation energies of clustering $Q$ for alloys 1 and 2 (Table 2) reveal significant higher values for the Sn-added material.

As found by Seyedrezai et al. [12] for resistivity measurements in an Al-0.5%Mg-1%Si alloy, also for age hardening curves during NA of AA6061 with and without Sn up to three stages of linear logarithmic hardening are perceived (Figure 1 to Figure 3). In contrast to alloy 1, stage I lasts for the Sn added alloys 2 and 3 for a long period of time. This can be explained by atom probe tomography measurements performed in [3]: Before the onset of hardening in stage II, Sn added alloys show random distributions of the solute atoms in the Al matrix and thus no clusters can contribute to the hardness until this time of NA.

As discussed in the introduction, Seyedrezai et al. [12] observed only a slight influence of the STT (525 °C and 560 °C) on kinetics of clustering, which was expressed also by comparable activation energies $Q$. For alloy 1, the calculated effective activation energies $Q$ at the onset of stage II after a SHT at 530 °C and 570 °C (Table 2) are also comparable. Although the actual values differ slightly from the $Q$ values obtained by Seyedrezai et al., they remain in the range of activation energies reported in literature (~53.5 kJ/mol found by Gaber et al. [18]). Furthermore, a possible influence of the alloy composition on $Q$ cannot be excluded.

In the following possible reasons for the significantly higher $Q$ values for the Sn-added alloy 2 compared to the Sn-free alloy 1 are discussed (Table 2). As shown in the introduction, Sn reduces the amount of vacancies in the matrix available for diffusional processes of other alloying elements (like Mg or Si) due to the formation of Sn-vacancy pairs. Thus, clusters of stage II form at a much slower rate than in alloys without Sn. The higher $Q$ values for alloy 2 let assume a direct influence of Sn on clustering kinetics. Thermally activated release of vacancies from Sn-vacancy complexes with increasing temperature may give an additional contribution to $Q$ (which is normally attributed to the migration of solutes barrier only) associated with the Sn-vacancy binding energy. Besides this, another possible explanation may be an additional thermally activated contribution of the migration for Sn-vacancy pairs or small complexes to the effective activation energy of clustering $Q$.

## Conclusions

The objective of this study was to analyze the influence of varying NA temperatures between 5 and 45 °C and two STTs (530 °C and 570 °C) on NA hardening kinetics for a Sn-free commercial Al-Mg-Si alloy compared to two Sn-added alloys containing different Mg-, Si- and Cu-amounts.

Up to three different stages of hardening could be observed for the alloys investigated. For the commercial, Sn-free, variant stage I is not observed at 45 °C, but might occur at shorter times than investigated.

For the commercial alloy and both STTs, comparable effective activation energies of clustering $Q$ are calculated at the onset of hardening during NA.

Sn-addition results in higher activation energy values of clustering $Q$ than obtained for the Sn-free reference alloy. Additional contributions from the migration energy for the migration of Sn-vacancy pairs or a thermally activated release of vacancies are assumed as possible explanations for this effect.

**Acknowledgment**

The authors wish to express their sincere thanks to the Austrian Research Promotion Agency (FFG) and the AMAG Rolling for their financial support of this work.

**References**

1. F. Ostermann, *Anwendungstechnologie Aluminium*, 2nd ed. (Springer, 2007).
2. S. Pogatscher, H. Antrekowitsch, H. Leitner, T. Ebner, and P. Uggowitzer, "Mechanisms controlling the artificial aging of Al-Mg-Si Alloys," Acta Materialia **59**, 3352–3363 (2011).
3. S. Pogatscher, H. Antrekowitsch, M. Werinos, F. Moszner, S. Gerstl, M. F. Francis, W. A. Curtin, J. F. Löffler, and P. J. Uggowitzer, "Diffusion on Demand to Control Precipitation Aging: Application to Al-Mg-Si Alloys," Phys. Rev. Lett. **112**, 225701–225705 (2014).
4. J. Banhart, C. Chang, Z. Liang, N. Wanderka, M. Lay, and A. Hill, "Natural aging in Al-Mg-Si alloys - A process of unexpected complexity," Advanced Engineering Materials **12**, 559–571 (2010).
5. I. Kovaćs, J. Lendvai, and E. Nagy, "The mechanism of clustering in supersaturated solid solutions of A1-$Mg_2Si$ alloys," Acta Metallurgica **20**, 975–983 (1972).
6. Brenner, P., Kostron, H., "Über die Vergütung der Aluminium–Magnesium–Silizium–Legierungen (Pantal)," Zeitschrift für Metallkunde **4**, 89–97 (1939).
7. J. Banhart, M. Lay, C. Chang, and A. Hill, "Kinetics of natural aging in Al-Mg-Si alloys studied by positron annihilation lifetime spectroscopy," Physical Review B **83**, 014101 (2011).
8. S. Esmaeili and D. Lloyd, "Modeling of precipitation hardening in pre-aged AlMgSi(Cu) alloys," Acta Materialia **53**, 5257–5271 (2005).
9. H. Zandbergen, S. Andersen, and J. Jansen, "Structure determination of $Mg_5Si_6$:particles in Al by dynamic electron diffraction studies," Science **277**, 1221–1225 (1997).
10. S. Pogatscher, H. Antrekowitsch, H. Leitner, D. Pöschmann, Z. Zhang, and P. Uggowitzer, "Influence of interrupted quenching on artificial aging of Al-Mg-Si alloys," Acta Materialia **60**, 4496–4505 (2012).
11. M. Werinos, H. Antrekowitsch, W. Fragner, T. Ebner, P. Uggowitzer, and S. Pogatscher, *Influence of Sn-solubility on suppression of natural aging in an AA6061 aluminum alloy.* (Paper presented at MS&T '14, Pittsburgh, USA, 2014).
12. H. Seyedrezai, D. Grebennikov, P. Mascher, and H. Zurob, "Study of the early stages of clustering in Al-Mg-Si alloys using the electrical resistivity measurements," Materials Science and Engineering A **525**, 186–191 (2009).
13. R. C. Picu and D. Zhang, "Atomistic study of pipe diffusion in Al-Mg alloys," Acta Materialia **52**, 161–171 (2004).
14. S. Pogatscher, E. Kozeschnik, H. Antrekowitsch, M. Werinos, S. Gerstl, J. F. Löffler, and P. Uggowitzer, "Process-controlled suppression of natural aging in an Al-Mg-Si alloy," Scripta Materialia **89**, 53–56 (2014).
15. S. Pogatscher, M. Werinos, and Antrekowitsch, H. and Uggowitzer, P.J., "The role of vacancies in the aging of Al-Mg-Si alloys," Materials Science Forum **794-796**, 1008–1013 (2014).
16. Z. Guo, W. Sha, and E. A. Wilson, "Modelling of precipitation kinetics and age hardening of Fe-12Ni-6Mn maraging type alloy," Materials Science and Technology **18**, 377–382 (2002).
17. A. Juhász, I. Kovács, J. Lendvai, and P. Tasnádi, "Initial clustering after quenching in AlZnMg alloys," Journal of Materials Science **20**, 624–629 (1985).
18. A. Gaber, K. Matsuda, Z. Yong, T. Kawabata, A. M. Ali, and S. Ikeno, "DSC and HRTEM Study of Precipitation in Al-Mg-Si-Cu Alloys," Materials Forum **28**, 402–405 (2004).